PHYSICAL REVIEW C

NUCLEAR PHYSICS

THIRD SERIES, VOLUME 53, NUMBER 3 **MARCH 1996**

RAPID COMMUNICATIONS

The Rapid Communications section is intended for the accelerated publication of important new results. Manuscripts submitted to this section are given priority in handling in the editorial office and in production. A Rapid Communication in **Physical Review C** *may be no longer than five printed pages and must be accompanied by an abstract. Page proofs are sent to authors.*

Reaction mechanisms in $^{12}C(\gamma,pp)$ near 200 MeV

E. D. Hackett, W. J. McDonald, A. K. Opper, M. A. Quraan, N. L. Rodning, and F. M. Rozon
Centre for Subatomic Research, University of Alberta, Edmonton, Alberta, Canada T6G 2N5

G. Feldman, N. R. Kolb, R. E. Pywell, D. M. Skopik, D. E. Tiller, and J. M. Vogt
Saskatchewan Accelerator Laboratory, University of Saskatchewan, Saskatoon, Saskatchewan, Canada S7N 5C6

E. Korkmaz and G. V. O'Rielly
Physics Department, University of Northern British Columbia, Prince George, British Columbia, Canada V2N 4Z9

(Received 25 September 1995)

Inclusive $^{12}C(\gamma,pp)$ cross sections have been measured with tagged photons in the range E_γ=187–227 MeV using the Saskatchewan-Alberta Large Acceptance Detector (SALAD). The large angular acceptance allowed the measurement of noncoplanar *pp* emission. The cross sections were compared to a Monte Carlo intranuclear cascade calculation. Agreement was reasonable for the shapes of the cross sections but the calculated total cross section was 3.9 times larger than the data.

PACS number(s): 25.20.−x, 21.30.Fe, 23.20.En

The combination of a large acceptance detector and a tagged photon beam has made it possible for the first time to measure $^{12}C(\gamma,pp)$ cross sections with complete energy and angular distributions, including previously unmeasured out-of-plane *pp* coincidence cross sections [1]. These data should provide a much more stringent test of theoretical models of multinucleon emission than previous inclusive (γ,N) experiments.

The mechanisms leading to the photon-induced emission of multiple nucleons are not well understood. Many (γ,NN) experiments have concentrated on (γ,np), which is dominated by dipole $(E1)$ absorption. Cross sections for *direct* (γ,pp) are roughly an order of magnitude smaller, since the absorption of the photon can only proceed through the weaker neutral pion-exchange diagrams. The suppression of the strong charged meson-exchange diagrams for (γ,pp) implies that the reaction must proceed via other reaction mechanisms: quadrupole and higher-order multipole absorption on a *pp* pair, absorption on a *np* pair followed by *NN* rescattering, or real pion production followed by pion absorption on a *NN* pair. The latter two processes are driven by final-state interactions (FSI) which make it difficult to study the initial photon interaction vertex. These three mechanisms may not account for the complete (γ,NN) cross section, in which case other more interesting mechanisms may contribute significantly. These include short-range *NN* correlations, ΔN interactions, or three-body forces. All three of these mechanisms represent a significant refinement or departure from the presently accepted models of *NN* interactions.

The large number of competing processes makes detailed theoretical calculations intractable. Microscopic calculations of both $(\gamma,\pi N)$ and (γ,NN) interactions are at an early stage. Qualitative agreement with data has been obtained with intranuclear cascade models, which use a Monte Carlo technique to simulate all the interactions in the nucleus [2]. There is a need for coincidence experiments with complete angular distributions, to disentangle the many possible reaction mechanisms.

The data were taken using the Saskatchewan-Alberta Large Acceptance Detector (SALAD) at the Saskatchewan Accelerator Laboratory (SAL). The experiment used tagged photons in the range E_γ=187–227 MeV to measure inclusive $^{12}C(\gamma,pp)$ cross sections. An electron beam of 290 MeV and ~45% duty factor was incident on a 115 μm aluminum radiator producing bremsstrahlung photons. The photons were tagged via the standard photon tagging technique using the SAL photon tagger [3]. The average tagged photon flux was 2×10^6 photons/s integrated over the photon energy

range. The tagging efficiency was measured approximately every 24 h during the experiment by using a lead glass Čerenkov detector directly in the beam to detect photons in coincidence with electrons in the focal plane. The photon flux from the accelerator was too intense for the Čerenkov detector and was reduced by 3 orders of magnitude in order to perform these measurements. Tests have been performed that show the measured efficiency is insensitive to the photon flux in the range of interest in this experiment. The tagging efficiency was approximately 55%.

SALAD [4] consists of four cylindrical wire chambers surrounded by a plastic scintillator calorimeter segmented into 24 ΔE-E telescopes. A high-pressure cylindrical gas target cell is placed along the axis of the detector. The target, wire chambers, and calorimeter are designed to minimize energy loss as well as dead areas in the detector.

Data for ^{4}He were taken simultaneously with the ^{12}C data. At the beginning of the run the target was filled with ^{4}He gas at 714 kPa pressure. The carbon targets were in the form of three solid polyethylene disks, which had an average thickness of 1.58 ± 0.01 mm and a radius of approximately 30 mm, mounted inside the target cell. They were suspended, perpendicular to the beam, approximately at $z = 0, \pm 300$ mm, where z is the distance along the beam path from the center of the detector.

The SALAD trigger requirement was $\geqslant 2$ ΔE signals above a threshold and $\geqslant 2$ telescopes for which the sum of the E and ΔE signals was above another threshold. This *sum threshold* trigger was used to reject electron events and is described in Ref. [4]. A coincidence was then required between SALAD and the photon tagger electronics. An additional software condition was placed on the coincidence TDC spectrum to select ''true'' events.

The data were analyzed using tracking information from the SALAD wire chambers as well as ΔE-E information from the calorimeter. For events which had tracks, the *minimum distance* between two tracks was defined as the shortest line segment joining the tracks. The vertex was then defined as the midpoint of this line segment. Cuts were applied to the minimum distance between the tracks (<40 mm) and the radial position of the vertex (<60 mm) to select events with a two-track vertex.

The energy deposition in the calorimeter was used to determine the particle type associated with each track. The stopping power (dE/dx) vs energy (E) was linearized using

$$PID \equiv \frac{[(E+\Delta E)^{\alpha} - E^{\alpha}]}{\alpha D \Delta x} \simeq z^2 A, \tag{1}$$

where Δx is the path length through the ΔE scintillator and the constants D and α were fitted to proton data. Since this is an approximation, PID is only roughly equal to z^2A and a scaling factor was added such that $PID = 1$ for protons. Figure 1 is a two-dimensional plot of particle type for events with two tracks from a vertex. The data are sorted such that the larger value appears on the x axis and the smaller on the y axis. Events corresponding to (γ,pp) are clearly seen, as well as (γ,pd) and $(\gamma,p\pi)$. Since the channels are not cleanly separated by particle identification, corrections must be made for misidentification of particle type. Misidentification of protons is taken care of in the Monte Carlo simulation, which is used to determine the detection efficiency, since identical cuts are applied to the simulation and the data. However, a correction must be made for pions and deuterons misidentified as protons. By fitting the PID spectra it was determined that misidentified particles gave an 11% contribution in the proton peak. A correction for this was made by multiplying the (γ,pp) yields by a constant factor.

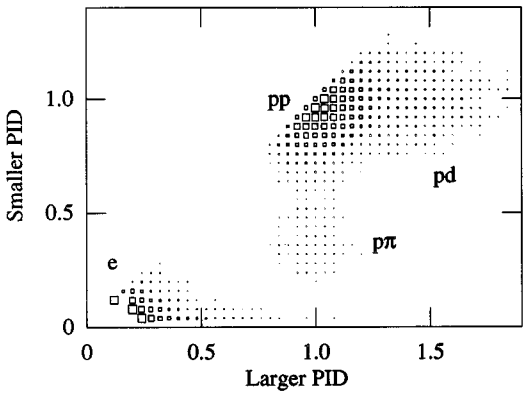

FIG. 1. Two-dimensional histogram of particle identification for two-track events in SALAD. Events are identified as (γ,pp), (γ,pd), and $(\gamma,p\pi)$. Electrons are located in the lower left corner of the plot.

The minimum proton energy threshold for SALAD was $T_p = 28$ MeV at the event vertex for $\theta = 90°$. To avoid sensitivity to the precise placement of the threshold, a software threshold was applied at $T_p = 34$ MeV.

Cuts were placed on the z position of the event vertex to select only ^{12}C events [the hydrogen in the solid target being unable to contribute via (γ,pp)]. A correction was made for ^{4}He(γ,pp) events within the ^{12}C cuts. Since the distributions for ^{4}He(γ,pp) events were found to be very similar to those for ^{12}C(γ,pp), the ^{12}C yields were simply multiplied by 0.91 to correct for the inclusion of ^{4}He events.

The final step in the analysis was the subtraction of random coincidences between the photon tagger and SALAD. The random contribution was determined from the yield on either side of the coincidence peak in the TDC spectrum to be 11%.

Once the yield of events for a specific reaction, N, is known, the differential cross section for the reaction can be calculated with respect to any selected variable, q_j, as

$$\frac{d\sigma}{dq_j} = \frac{N}{N_\gamma N_T \epsilon dq_j}. \tag{2}$$

Here, N_γ and N_T are the number of incident photons and the number of target nuclei, respectively. The yield, cross section, and efficiency are all functions of the kinematic variables which specify the reaction. The integrated flux is given by $N_\gamma = N_e \times \epsilon_{\text{tag}}$, where N_e is the total number of electrons striking the tagger focal plane and ϵ_{tag} is the average tagging efficiency.

In Eq. (2), the factor ϵ is the effective efficiency of the detector, which is the convolution of the intrinsic efficiency and the geometric acceptance of SALAD, and is calculated using a Monte Carlo simulation. The technique of determining ϵ involves three steps: (1) events are generated which

satisfy the kinematics for the desired reaction, (2) the detector response to these events is simulated, and (3) the *simulated* data are analyzed, with exactly the same software and cuts. The detector efficiency is calculated as the ratio of detected events to generated events. Provided that the Monte Carlo simulation faithfully reproduces the detector response, the calculated efficiency is accurate.

The efficiency depends on the energies E_1 and E_2 of the two protons as well as their angles θ_1, θ_2, ϕ_1, and ϕ_2. Integrating over ϕ_1 or ϕ_2, the kinematics are specified with five variables: $\epsilon=\epsilon(E_1,E_2,\cos(\theta_1),\cos(\theta_2),\Delta\phi)$. The detected and generated $^{12}C(\gamma,pp)$ events are binned according to the five variables and the detector efficiency is determined bin by bin. The fivefold differential cross section is then given by

$$\frac{d^5\sigma}{dE_1 dE_2 d\cos(\theta_1) d\cos(\theta_2) d\Delta\phi} = \frac{N(E_1,E_2,\cos(\theta_1),\cos(\theta_2),\Delta\phi)}{N_\gamma N_T \epsilon(E_1,E_2,\cos(\theta_1),\cos(\theta_2),\Delta\phi)(\Pi_j \Delta q_j)}, \quad (3)$$

where $q_j = E_1$, E_2, $\cos(\theta_1)$, $\cos(\theta_2)$, or $\Delta\phi$. Single-differential cross sections are determined by integrating over the other variables.

The major sources of systematic error in the normalized cross sections were tagging efficiency (2%), particle misidentification (3%), ^{4}He backgrounds (2%), energy loss in the detector (2%), and tracking efficiency (5%). The errors, combined in quadrature, give a total systematic error of 7%.

Calculating the $^{12}C(\gamma,pp)$ cross section is complicated due to the many different reaction channels which can contribute. The data are inclusive with respect to undetected protons, neutrons, or other charged particles which were outside the detector acceptance or below threshold. In addition to direct absorption on two or more nucleons, pion photoproduction can also produce a two-proton final state. A pion produced in the nucleus has a large probability of being scattered or absorbed, exciting more nucleons. In addition, any nucleons produced are subject to rescattering which will alter their energy and angular distribution and may excite and emit other nucleons. A full quantum mechanical treatment of all these processes is intractable.

To circumvent this problem, a traditional approach is the Monte Carlo intranuclear cascade calculation. An intranuclear cascade calculation by Carrasco *et al.* [5] has been compared to the $^{12}C(\gamma,pp)$ data of the current experiment. This particular theoretical treatment has the advantage of separability of the contributions from different reaction channels. In addition, final-state interactions (FSI) are accurately treated with a Monte Carlo technique which makes it easier to apply experimental energy thresholds to the calculated cross sections.

Reaction probabilities for photons, pions, and nucleons are obtained from true microscopic calculations of these elementary processes. Carrasco and Oset [2] give a full description of the microscopic calculation of the total photon absorption cross section. After the primary photon interaction, excited nucleons and pions are propagated as classical particles. The nucleons and pions are excited from a Fermi sea which does not respect the shell structure of the target nucleus. Thus, separation energies must be put in explicitly. At each Monte Carlo step, the reaction probability is evaluated and further nucleons may be excited via pion absorption, pion scattering, or NN scattering. The Monte Carlo propagation of nucleons induces large uncertainty for low-momentum particles [6], which imposes a minimum proton vertex energy for reliable FSI calculation. The present calculation used a cutoff of 28 MeV.

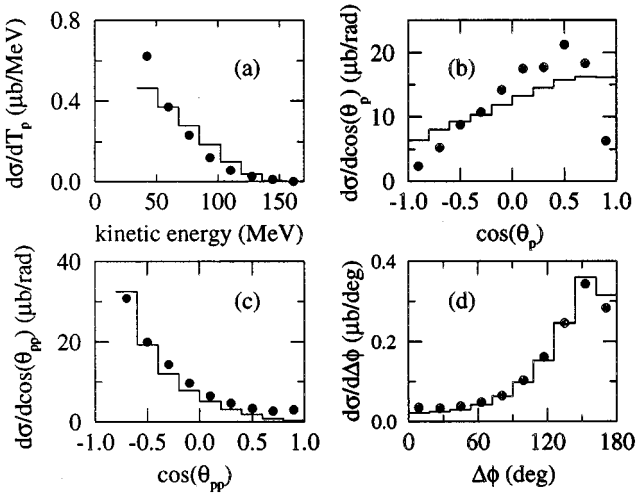

FIG. 2. Comparison of differential cross section data (filled circles) with the calculation of Carrasco *et al.* (solid histogram) as a function of the proton kinetic energy T_p (a), cosine of the proton angle θ_p (b), cosine of the opening angle θ_{pp} (c), and phi difference $\Delta\phi$ (d). The theoretical curves have been divided by 3.9. The error bars are smaller than the plot symbols and are a combination of the statistical error in the yield and the nonsystematic error in the detection efficiency.

Before comparing data and theory, the results of the calculation must be modified to reflect the angular acceptance and the energy threshold of the SALAD detector. This is accomplished by setting the calculated cross section to zero in any bin where the efficiency of the SALAD detector, $\epsilon(E_1,E_2,\cos(\theta_1),\cos(\theta_2),\Delta\phi)$, is identically zero. In this way the theoretical calculation is limited to the same phase space as the experimental data.

Integrating the data, one obtains a total cross section of 24.5 ± 0.1 μb while the calculation gives 95.8 ± 0.1 μb, a factor of 3.9 discrepancy. The error on the data is a combination of the statistical error in the yield and the nonsystematic error in the detection efficiency. The error on the calculation reflects the statistics of the Monte Carlo calculation. Previous SALAD experiments have reproduced known cross sections using the same Monte Carlo method to calculate detector efficiency [7]. Both the ^{3}He(γ,pd) and the well-known $D(\gamma,p)n$ cross sections have been reproduced to within 10%. The SALAD $^{12}C(\gamma,pp)$ cross section agrees with a previous experiment [8], but large statistical errors make this agreement approximate and the comparison can only be made over a small fraction of phase space.

Figure 2 shows the differential cross sections for the kinetic energy of the proton T_p (a), cosine of the proton angle θ_p (b), cosine of the opening angle between the two protons θ_{pp} (c), and phi difference between the two protons $\Delta\phi$ (d). The calculations have been scaled down by the factor of 3.9.

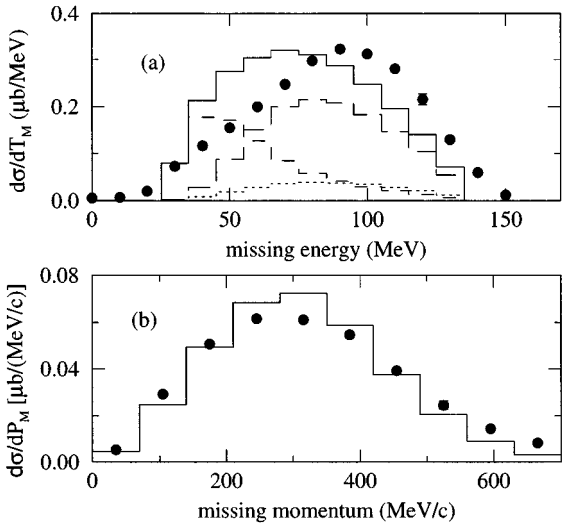

FIG. 3. Comparison of differential cross section as a function of missing energy (a) and missing momentum (b) for data (filled circles), full calculation (solid histogram), pp absorption (short-dashed histogram), and np absorption (long-dashed histogram). The dotted histogram is the sum of quasifree absorption on three nucleons and pion production followed by reabsorption. The theoretical calculations of missing energy have been shifted by 27 MeV (see text). The theoretical curves have been divided by 3.9. The error bars, typically smaller than the plot symbols, are a combination of the statistical error in the yield and the nonsystematic error in the detection efficiency.

The shape of the $d\sigma/dT_p$ and $d\sigma/d\cos(\theta_p)$ distributions in Figs. 2(a) and 2(b) gives reasonable agreement. The agreement is excellent for the angular distributions in $\cos(\theta_{pp})$ and $\Delta\phi$ in Figs. 2(c) and 2(d). The dip in $d\sigma/d\Delta\phi$ near $\Delta\phi = 180°$ is caused by a cut, $\theta_{pp}<150°$, placed on the data. As the opening angle between the two tracks becomes large, the position of the vertex is poorly defined. In the limit of back-to-back or parallel tracks, the vertex position is completely undefined. To eliminate this uncertainty, in this first report of our results, events with opening angles greater than 150° were rejected. This excluded 25% of the data.

In order to gain insight into the mechanisms responsible for two proton emission, it is useful to calculate the missing energy, $T_M \equiv T_\gamma - T_1 - T_2$ where T_γ is the photon energy and T_1 and T_2 are the kinetic energies of the two protons. Figure 3(a) compares the data to the calculated missing energy spectrum (solid histogram). The calculations have been scaled down by the factor of 3.9. It also shows the contributions to the cross section from each of the primary photon absorption processes: NN absorption (split into np and pp channels), $3N$ absorption and pion production followed by reabsorption of the pion by 2 or 3 nucleons. Either directly or through rescattering, these three processes can lead to two protons being emitted with enough energy to be detected in SALAD. The missing energy spectra from the calculation of Carrasco *et al.* are shifted by 27 MeV in a rough attempt to account for the lowest separation energy (p-p shell) of two protons from ^{12}C. This does not deal properly with protons from p-s or s-s shells or events in which other undetected nucleons are emitted. Significant strength from quasifree pp absorption seems to be ruled out due to the shape; however, putting in proper separation energies for the nucleons would tend to shift some of this distribution to higher missing energies. This makes it impossible to separate quasifree absorption kinematics from the other contributions on the basis of the energy correlations.

The theory suggests that the bulk of the cross section is due to quasifree np absorption followed by a final-state interaction that produces two protons above detector thresholds. The prospects, at this time, of extracting information on NN correlations from such a process seem doubtful.

The theory predicts that only a small portion of the cross section at these energies is due to photopion production followed by the reabsorption of the pion. Thus, for this measurement, the missing momentum ($\mathbf{P}_M \equiv \mathbf{P}_\gamma - \mathbf{P}_1 - \mathbf{P}_2$) distribution is not expected to be a measure of the initial momentum of a NN pair in the target nucleus. Instead, the missing momentum is determined by the dynamics of the final state in the way in which energy and momentum are shared.

Figure 3(b) compares the data to the calculated missing momentum spectrum. Again the calculation has been scaled down by the factor of 3.9. The shape of the calculation is consistent with the measurement. The missing momentum of the two protons is too low for a single undetected nucleon in the final state to explain the large missing energy. Thus, two or more undetected nucleons must be emitted in the reaction.

These comparisons show that the shape of the distributions for ^{12}C(γ,pp) is well described by the calculations although the discrepancy in absolute magnitude is large. Though the calculation of Carrasco *et al.* [5] is very good at isolating the contribution of a given mechanism, the final cross section it produces is an incoherent sum of all these mechanisms. If interference between the pp and np absorption channels is important, this will be absent in the calculated cross section.

Boffi and Giannini [9] have suggested that the effect of strong short-range correlations would be to decrease the magnitude of the (γ,NN) cross section by a factor of up to 100, without significantly modifying the angular distribution. Even a much more modest decrease in the calculated cross section would greatly improve the agreement with the data.

In conclusion, we have measured ^{12}C(γ,pp) cross sections using tagged photons and a large acceptance detector and compared the data to an intranuclear cascade model. The most striking disagreement (a factor of 3.9) between theory and experiment is in the size of the total cross section for ^{12}C(γ,pp) for the range of photon energies $E_\gamma = 187$–227 MeV. In general, a simple model, such as the impulse approximation, overestimates the cross section. Refining the model invariably lowers the cross section as interference effects and final-state interactions are added. The model of Carrasco *et al.* already represents a significant refinement of earlier intranuclear cascade methods, but perhaps future refinements may decrease its predicted total cross section. Given the large effect predicted by Boffi and Giannini [9], the inclusion of NN correlations may prove worthwhile.

The authors would like to thank R.C. Carrasco for supplying the computer code for the theoretical calculations. This work was supported by the Natural Sciences and Engineering Research Council of Canada.

[1] E.D. Hackett, Ph.D. thesis, University of Alberta, 1995.
[2] R.C. Carrasco and E. Oset, Nucl. Phys. **A536**, 445 (1992).
[3] J.M. Vogt, R.E. Pywell, D.M. Skopik, E.L. Hallin, J.C. Bergstrom, H.S. Caplan, K.I. Blomqvist, W. Del Bianco, and J.W. Jury, Nucl. Instrum. Methods Phys. Res. Sect. A **324**, 198 (1993).
[4] E.B. Cairns *et al.*, Nucl. Instrum. Methods Phys. Res. Sect. A **321**, 109 (1992).
[5] R.C. Carrasco, M.J. Vicente Vacas, and E. Oset, Nucl. Phys. **A570**, 701 (1994).
[6] L.L. Salcedo, E. Oset, M.J. Vicente-Vacas, and C. Garcia-Recio, Nucl. Phys. **A484**, 557 (1988).
[7] N.R. Kolb *et al.*, Phys. Rev. C **49**, 2586 (1994).
[8] M. Kanazawa, S. Homma, M. Koike, Y. Murata, H. Okuno, F. Soga, N. Yoshikawa, and A. Sasaki, Phys. Rev. C **35**, 1828 (1987).
[9] S. Boffi and M.M. Giannini, Nucl. Phys. **A533**, 441 (1991).